Monitoring of Winter Wheat Biomass Using UAV Hyperspectral Texture Features

Chang Liu[1,2,3,4], Guijun Yang[2,3,4], Zhenhai Li[2,3,4(✉)], Fuquan Tang[1], Haikuan Feng[2,3,4], Jianwen Wang[2,3,4], Chunlan Zhang[1,2,3,4], and Liyan Zhang[2,3,4]

[1] College of Geomatics, Xi'an University of Science and Technology, Xi'an, China
l224l29134@qq.com, fuquantang@l63.com, l964362790@qq.com

[2] Key Laboratory of Quantitative Remote Sensing in Agriculture of Ministry of Agriculture P. R. China, Beijing Research Center for Information Technology in Agriculture, Beijing, China
guijun.yang@l63.com, lizh323@l26.com, fenghaikuanl23@l63.com, 985764715@qq.com, 344014704@qq.com,

[3] National Engineering Research Center for Information Technology in Agriculture, Beijing, China

[4] Beijing Engineering Research Center for Agriculture Internet of Things, Beijing, China

Abstract. Biomass is an important indicator to evaluate vegetation life activities and hyperspectral imagery from unmanned aerial vehicle (UAV) supplied with abundant texture features shows a great potential to estimate crop biomass. In this paper, principal component analysis (PCA) was used to select the principal component bands from UAV hyperspectral image. Eight texture features from the principal component bands were extracted by Gray Level Co-occurrence Matrix method, and the sensitive texture features were finally selected to construct the biomass estimation model. The results show that: (1) Texture features mean, ent, sm, hom, con, dis of the first principal component (pca1) and the mean of the third principal component (pca3) were significantly correlated with the biomass. (2) The biomass model by multiple texture features (R^2 = 0.654, RMSE = 0.808 (10^3 kg/hm^2)) demonstrated better fitting effect than that by single texture feature (R^2 = 0.534, RMSE = 0.960 (10^3 kg/hm^2)). The biomass estimation model based on the texture features of multiple principal components had a good fitting effect. Therefore, texture features of the UAV platform can accurately predict the winter wheat biomass.

Keywords: Hyperspectral image · Texture feature · Biomass Principal component

D. Li and C. Zhao (Eds.): CCTA 2017, IFIP AICT 546, pp. 241–250, 2019.
https://doi.org/10.1007/978-3-030-06179-1_25

1 Introduction

Biomass is an important indicator to evaluate vegetation life activities and can be used as an important basis for growth monitoring and remote sensing estimation [1, 2]. The traditional method of biomass acquisition is not only destructive, consuming time and energy, but also difficult to achieve large area monitoring [3]. In recent years, hyperspectral remote sensing has been widely used in quantitative remote sensing of vegetation biomass with its advantages of timely, non-destructive, large monitoring area and high spectral resolution [3]. Many researchers have used satellite and the other remote sensing data to study the estimation of vegetation biomass. Chen et al. [4] using HJ-1C images, constructed a biomass estimation model based on the common vegetation index of NDVI, OSAVI, MSAVI, SAVI, MTVI2, finally, the result showed that the biomass model based on MTVI2 has the best performance to estimate grassland biomass. Fan et al. [5] constructed a linear regression biomass model, a multivariate linear regression biomass model and a partial least squares regression biomass model using spectral feature that extracted from hyperspectral data, which indicates that the three models have a good fitting effect to estimate biomass with the R2 value of more than 0.9. The research of Gao et al. [6] showed that a multivariate regression biomass model constructed by TVI, MTVI2, GNDVI, NLI, MSR, RDVI and IPVI has a good inversion accuracy to shrubs. Satellite remote sensing technology can achieve large-scale remote sensing monitoring of agronomic parameter, however, the cycle time for acquiring data is long and the ground resolution of remote sensing image is not high enough, leading to a limited application in precision agriculture [7]. Meanwhile, the UAV platform for remote sensing technology, with the advantages of low maintenance costs, lightweight, flexible, can also obtain high spatial resolution and temporal resolution of remote sensing data, so it has become a hot topic in precision agriculture [8]. Yang [9] achieved biomass inversion of winter wheat based on the UAV platform laser radar technology. Zhang et al. [10] made use of UAV images to construct an estimation models between different vegetation index and grassland biomass, and the model constructed by NGRDI has a good fitting effect with the R2 value of 0.856. Lu et al. [11] obtained hyperspectral data through the UAV platform, and establish a stagewise estimation model of soybean biomass by spectral characteristics and plant height, which indicates a good fitting effect. Although many scholars has used spectral information for biomass inversion, but there was still saturation phenomenon exist. It is difficult to solve the above problems according to the simple spectral information, while, remote sensing technology based on UAV platform can obtain abundant texture information and can provide support for the retrieval of biomass. Nichol et al. [12] found that the accuracy of biomass estimation model based on AVNIR-2 and SPOT-5 multispectral data can be improved in combination with texture features compared to single spectral features. The results of Xu et al. [13] show that there was a strong correlation between texture features and biomass using Landsat 8 OLI multispectral image data. Mu et al. [14] indicated that texture features of vegetation indices have higher ability to estimate biomass than vegetation indices. Therefore, in this study, we attempted to use principal component analysis to transform the original hyperspectral image acquired by UAV platform, and extract texture feature from the principal component bands containing most of the information, then estimating winter wheat

biomass by texture features. This research provided a way for hyperspectral remote sensing estimation of biomass based on the UAV platform.

2 Materials and Methods

2.1 Study Area

Field experiment was conducted in the 2014–2015 winter wheat growing season at Xiaotangshan National Experiment Station for Precision Agriculture, Changping District, Beijing, China. Changping district has a moderate climate and four distinctive seasons, which is located in 40°00′–40°21′N, 116°34′–117°00′E with an altitude of 36 m. The previous crop is maize, and the type of soil is silt loam in the experiment field.

The experiment was designed with an orthogonal experiment of variety, nitrogen fertilization and irrigation (Fig. 1). Experiment area were divided into 48 plots and set to three replications. The two varieties of winter wheat were Jing9843 and Zhongmai175. Nitrogen fertilizer application rates included four levels, 0 kg/hm^2, 195 kg/hm^2, 390 kg/hm^2, 780 kg/hm^2. The irrigation included three levels, rainfall, normal irrigation with100 mm and excess irrigation with 200 mm.

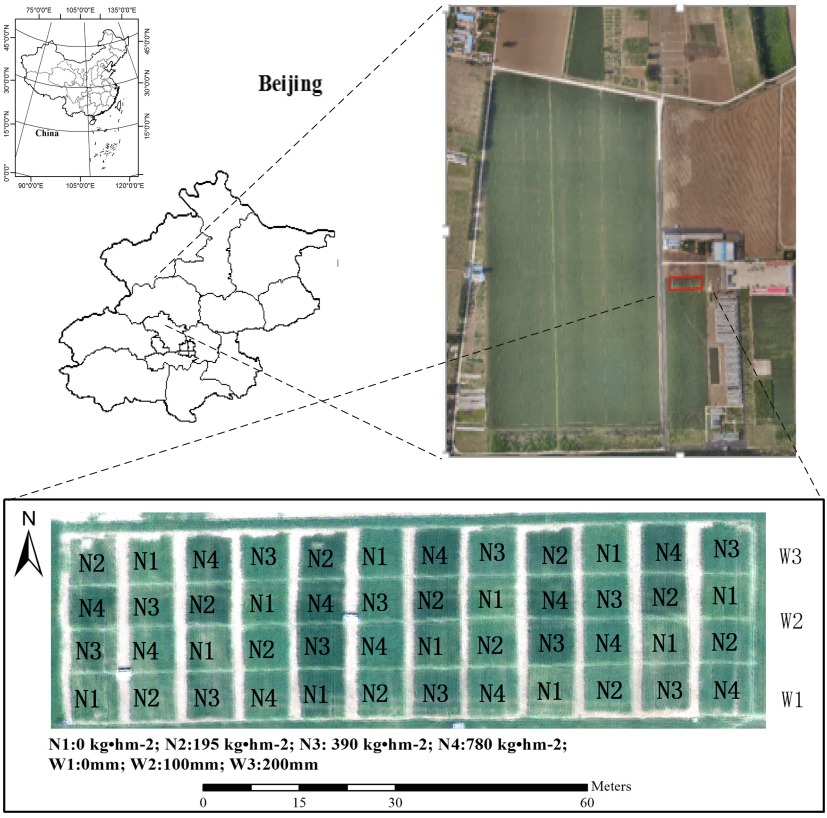

Fig. 1. Location of study area and experiment design

2.2 Field Measurements

Above ground biomass data was collected in the experiment at booting stage (26 April 2015) of winter wheat. A fixed area 0.3 m^2 was surveyed for the population density. 20 representative wheat tillers were selected from each plot. The samples were separated to stems and leaves, then stored in paper bags to be dried. Until the sub-organ samples became constant weight (about 24 h–48 h) in the oven, the dry weight of each sample can be obtained. Then biomass of winter wheat in per unit area was calculated by population density and dry weight of sample.

2.3 Hyperspectral Data and Pre-processing

Hyperspectral image at UAV platform (Fig. 2) was obtained at same time (April 26, 2015). The spectrometer was UHD 185, which is a new type of snapshot hyperspectral sensor and weighs 470 g. Its sensor can capture 450 nm–950 nm wavelengths with a sample interval of 4 nm. Finally, hyperspectral image and panchromatic image can be obtained both from the UHD 185.

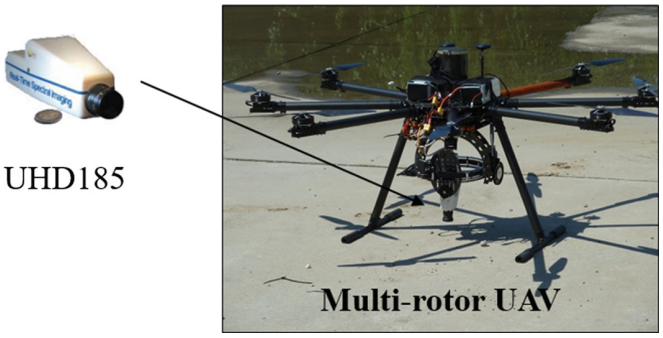

Fig. 2. UAV platform with UHD 185

According to the needs of this paper, we use Cubert-Pilot (Cubert, Germany) for image fusion of hyperspectral image and panchromatic images, and use Photoscan (Agisoft, Russia) for image stitching [15]. Then, the hyperspectral image was processed with ENVI software (Exelis Visual Information Solutions, USA) for radiation correction, atmospheric correction, and cutting [16].

2.4 Methods

The original hyperspectral image was transformed by principal component analysis, and the principal component bands containing much information were selected for texture analysis. Eight texture features, Mean, Variance, Homogeneity, Contrast, Dissimilarity, Entropy, Second Moment, and Correlation (Table 1) were extracted from the principal component bands at different window sizes ($3 \times 3, 5 \times 5, 7 \times 7, 9 \times 9,$. $11 \times 11, 15 \times 15, 21 \times 21$) by Gray Level Co-occurrence Matrix method. The region

of interest from texture images of different bands were extracted by ArcGIS 10.3.1 (Esri, USA), then texture feature values of the extracted regions were obtained. The biomass estimation model was constructed by the sensitive texture features after analyzing the correlation between texture features and above ground biomass using Pearson correlation analysis in SPSS 22.0 (IBM, USA).

Table 1. Texture features and its formulas in this study

Texture feature	Formulas
Mean (mean)	$mean = \sum_{i,j=0}^{N-1} iP(i,j)$
Variance (var)	$var = \sum_{i,j=0}^{N-1} iP_{i,j}(i - mean)^2$
Homogeneity (hom)	$hom = \sum_{i,j=0}^{N-1} i\frac{P_{i,j}}{1+(i-j)^2}$
Contrast (con)	$con = \sum_{i,j=0}^{N-1} iP_{i,j}(i-j)^2$
Dissimilarity (dis)	$dis = \sum_{i,j=0}^{N-1} iP_{i,j}\lvert i-j\rvert$
Entropy (ent)	$ent = \sum_{i,j=0}^{N-1} iP_{i,j}(-\mathrm{In}P_{i,j})$
Second Moment (sm)	$sm = \sum_{i,j=0}^{N-1} iP_{i,j}{}^2$
Correlation (corr)	$corr = \sum_{i,j=0}^{N-1} iP_{i,j}[\frac{(i-mean)(j-mean)}{\sqrt{var_i var_j}}]$

Note: $P(i,j) = \frac{V_{i,j}}{\sum_{i,j=0}^{N-1} V_{i,j}}$, where Vi, j represents the pixel brightness value of the (i, j)th element, and N represents the window size of the texture analysis.

3 Results

3.1 Selection of Texture Bands

As is shown in Fig. 3, the first three principal components explain more than 99% of the hyperspectral image (pca1, pca2, and pca3 contained 67%, 32% and 0.5% information of the hyperspectral image respectively), which can account for most of the variance of the original image. These principal components (pca1, pca2, pca3) were selected for texture features analysis.

3.2 Correlation Analysis Between Texture Features and Biomass

The relationship between principal components textures and biomass is shown in Table 2. Most of the texture features of pca1 were significantly correlated with biomass and the correlation coefficients(r) distributed between 0.5 and 0.7. Pca1_3_sm (representing texture feature 'sm' of pca1 band at the 3 × 3 window) was sensitive to biomass with r value of −0.673. As the window size changed, r values between texture features mean, hom, con, dis and biomass changed slightly. Mean of pca3 was significantly correlated to biomass with r value of 0.726, and other texture features of pca2, pca3 had a low correlation with biomass, which correlation coefficients were

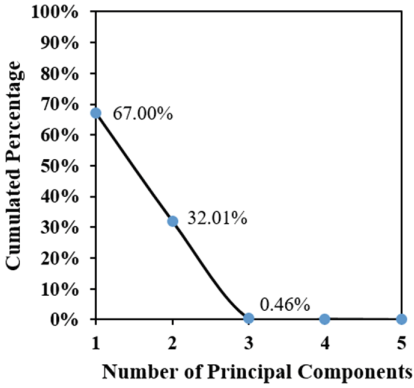

Fig. 3. Cumulated percentage variance in hyperspectral data of a number of PCs.

under 0.35. Therefore, pca1_3_mean, pca1_3_hom, pca1_3_con, pca1_3_dis, pca1_3_ent, pca1_3_sm, pca1_3_var, pca3_3_mean were selected as indexes of biomass estimation.

Table 2. Pearson's correlation coefficients(r) between texture features and biomass

Principle component	Window	Texture feature							
		mean	*ent*	*sm*	*var*	*hom*	*con*	*dis*	*corr*
pca1	3 × 3	−0.588*	0.657*	−0.673*	0.584*	−0.638*	0.600*	0.626*	−0.171
	5 × 5	−0.588*	0.639*	−0.664*	0.561*	−0.638*	0.600*	0.626*	−0.077
	7 × 7	−0.588*	0.628*	−0.656*	0.548*	−0.638*	0.600*	0.626*	−0.149
	9 × 9	−0.587*	0.621*	−0.648*	0.544*	−0.638*	0.600*	0.626*	−0.182
	11 × 11	−0.587*	0.619*	−0.645*	0.551*	−0.638*	0.600*	0.626*	−0.187
	15 × 15	−0.587*	0.621*	−0.646*	0.562*	−0.638*	0.600*	0.626*	−0.179
	21 × 21	−0.587*	0.631*	−0.655*	0.583*	−0.638*	0.600*	0.626*	−0.137
pca2	3 × 3	−0.134	−0.064	0.092	−0.086	0.035	−0.033	−0.035	−0.083
	5 × 5	−0.134	−0.135	0.171	−0.194	0.035	−0.032	−0.034	−0.407*
	7 × 7	−0.134	−0.193	0.232	−0.267	0.035	−0.032	−0.035	−0.465*
	9 × 9	−0.134	−0.231	0.272	−0.301	0.035	−0.033	−0.035	−0.482*
	11 × 11	−0.134	−0.248	0.293	−0.309	0.035	−0.033	−0.035	−0.486*
	15 × 15	−0.134	−0.238	0.295	−0.278	0.035	−0.033	−0.035	−0.476*
	21 × 21	−0.133	−0.218	0.284	−0.235	0.036	−0.033	−0.035	−0.443*
pca3	3 × 3	−0.726*	−0.257	0.258	−0.224	0.251	−0.230	−0.248	0.470*
	5 × 5	−0.726*	−0.256	0.257	−0.214	0.252	−0.230	−0.249	0.235
	7 × 7	−0.726*	−0.247	0.247	−0.198	0.252	−0.231	−0.249	0.203
	9 × 9	−0.726*	−0.227	0.225	−0.159	0.253	−0.231	−0.250	0.311
	11 × 11	−0.726*	−0.195	0.193	−0.096	0.253	−0.232	−0.250	0.338
	15 × 15	−0.726*	−0.108	0.107	0.081	0.254	−0.232	−0.251	0.438*
	21 × 21	−0.726*	−0.031	0.042	0.270	0.255	−0.233	−0.252	0.568*

Note: * It means the correlation is significant at 0.01 level.

3.3 Biomass Estimation Model by Single Texture Feature

Linear, power, logarithmic and exponential function were used to construct biomass model based on the selected texture features, and the best models were selected to show in Table 3. As is shown in Table 3, determination coefficients (R^2) of biomass estimation model are maintained at 0.4. The logarithmic function model based on texture pca3_3_mean has the best fitting effect with R^2 value of 0.534, RMSE value of 0.960 (10^3 kg/hm^2). The exponential function model based on texture pca1_3_sm has a R^2 value of 0.466, RMSE value of 0.806 (10^3 kg/hm^2) ranking the second (Fig. 4).

Table 3. Biomass estimation model by single texture feature

Principal component	Texture feature	Modeling equation	R^2	*RMSE* (10^3 *kg/hm*^{2})
pca1	*pca1_3_mean*	$y = 25.223e^{-0.094x}$	0.318	0.933
	pca1_3_ent	$y = 1.692x^{3.292}$	0.463	0.490
	pca1_3_sm	$y = 45.146e^{-7.366x}$	0.466	0.806
	pca1_3_var	$y = 12.801x^{1.163}$	0.396	0.889
	pca1_3_hom	$y = 1405.527e^{-7.839x}$	0.399	0.856
	pca1_3_con	$y = 7.356x^{1.258}$	0.409	0.875
	pca1_3_dis	$y = 14.062x^{1.948}$	0.428	0.849
pca3	*pca3_3_mean*	$y = 55.506-16.224\ln(x)$	0.534	0.960

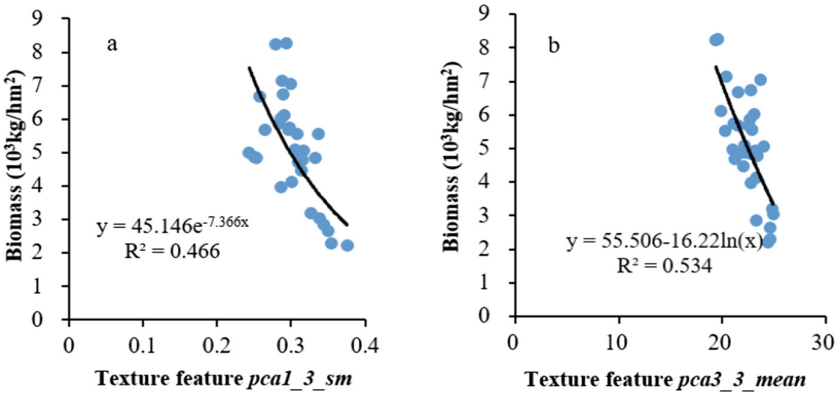

Fig. 4. Biomass estimation model by single texture feature; a. *pca1_3_sm*; b. *pca3_3_mean*;

3.4 Biomass Estimation Model by Multiple Texture Features

The biomass model based on the texture features of all principal components (Fig. 5) were built by multiple stepwise regression method. The R^2 and RMSE values between simulated and measured biomass were 0.654 and 0.808(10^3 kg/hm^2), respectively.

The results demonstrated that the fitting effect of biomass model based on multiple texture features is better than that by single texture feature. Texture information were

not completely taken into consideration when constructing the biomass model by single texture feature, while the biomass model based multiple texture features took advantage of several textures so that the estimation accuracy were improved. Using multiple texture features a potential prospect in estimating winter wheat biomass.

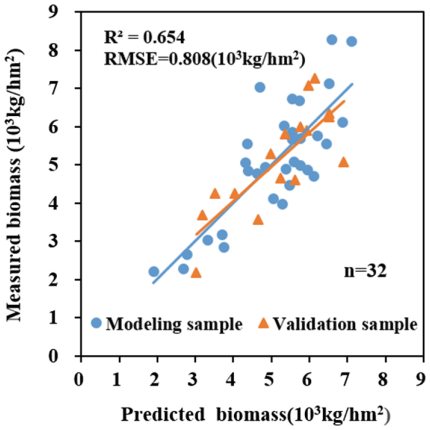

Fig. 5. Relationship between measured biomass and predicted biomass

3.5 Thematic Map of Winter Wheat Biomass

Thematic map of winter wheat biomass at booting stage was constructed by the biomass model based on the texture features of all principal components (Fig. 6). The map showed the winter wheat biomass of each plot in the experiment area. There were little biomass in the southwest and southeast, but much more biomass in the middle plots of the experiment area. The difference in biomass was resulted from different nitrogen fertilizer levels and irrigation levels. W3 treatment has higher biomass than W1 and W2 treatment, and W1 treatment has the lowest biomass. It is clear that sufficient irrigation

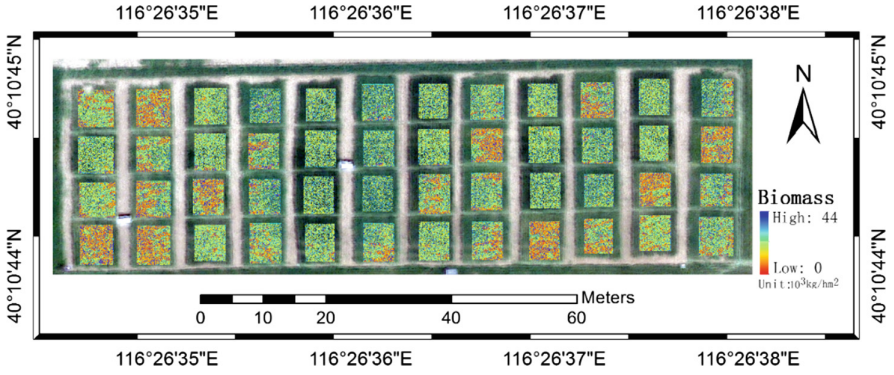

Fig. 6. Thematic map of winter wheat biomass at flagging stage

was beneficial for the growth of winter wheat biomass. N1 treatment had the lowest biomass. There was little difference between biomass of N2 and N3 treatment. When compared to N3 treatment, the biomass of N4 treatment increased slightly, sometimes it had no increase in biomass even decrease, which demonstrated that a suitable nitrogen fertilizer application rate can result in a faster grow in biomass of winter wheat.

4 Conclusions

In this study, the principal component bands were selected for texture feature analysis, and sensitive texture features that obtained from the principal component bands were used to construct the biomass estimation model. The results show that (1) *mean*, *ent, sm, hom, con, dis* of the first principal component (pca1) and the mean of the third principal component (pca3) were significantly correlated with the biomass at 0.01 level. (2) As the window size grows, the correlation coefficients between texture features *mean, hom, con, dis* and biomass changed slightly, which was almost stay in a steady state. (3) Biomass model by multiple texture features (R^2 = 0.654, RMSE = 0.808 (10^3 kg/hm^2)) demonstrates better fitting effect than that by single texture feature (R^2 = 0.534, RMSE = 0.960 (10^3 kg/hm^2)). The results suggest that the texture features of the UAV platform has a good application prospect in predicting winter wheat biomass, which can provide theoretical support and timely information for winter wheat growth monitoring and field production management.

Acknowledgments. This study was supported in part by the National Key Technologies of Research and Development Program (2016YFD0300602) and National Natural Science Foundation of China (Grant no. 61661136003, 41601346, 41471285, 441601346).

References

1. Du, X., Meng, J.H., Wu, B.F., et al.: Overview on monitoring crop biomass with remote sensing. Spectrosc. Spectr. Anal. **30**(11), 3098–3102 (2010)
2. Zhang, K., Wang, R.Y., Wang, X.P., et al.: Hyperspectral remote sensing estimation models for above ground fresh biomass of spring wheat on Loess Plateau. J. Chin. J. Ecol. **28**(6), 1155–1161 (2009)
3. Zhuang, D.Y., Li, W.G., Wu, L.Q.: Estimating winter wheat biomass based on satellite remote sensing. J. Arid Land Resour. Environ. **27**(10), 158–162 (2013)
4. Chen, P.F., Wang, J.L., Liao, X.Y., et al.: Using data of HI-1A/B Satellite for hulunbeier grassland aboveground biomass estimation. J. Nat. Resour. **25**(7), 1122–1131 (2010)
5. Fan, Y.B., Zhao, W.J., Gong, Z.N., et al.: Inversion methods for above-ground dry biomass of phragmites australis and typha angustifolia based on hyperspectral information. Wetl. Sci. **14**(5), 654–664 (2016)
6. Gao, M.L., Gong, Z.N., Zhao, W.J., et al.: The study of vitex negundo shrubs canopy biomass inversion in Beijing Jundu mountainous area based on vegetation indices. Acta Ecol. Sin. **34**(5), 1178–1188 (2014)

7. Gao, L., Yang, G.J., Wang, B.S., et al.: Soybean leaf area index retrieval with UAV (unmanned aerial vehicle) remote sensing imagery. Chin. J. Eco-Agric. **23**(7), 868–876 (2015)
8. Li, C.C., Niu, Q.L., Yang, G.J., et al.: Estimation of leaf area index of soybean breeding materials based on UAV digital images. Trans. Chin. Soc. Agric. Mach. **48**(8), 147–158 (2017)
9. Yang, F.: Estimation of winter wheat aboveground biomass with UAV LiDAR and hyperspectral data. Xi'an University of science and technology, Shaanxi (2017)
10. Zhang, Z.J., Li, A.N., Bian, J.H., et al.: Estimation aboveground biomass of grassland in zoige by visible vegetation index derived from unmaned aerial vehicle image. Remote Sens. Technol. Appl. **31**(1), 51–62 (2016)
11. Lu, G.Z., Yang, G.J., Zhao, X.Q., et al.: Inversion of soybean fresh biomass based on multi-payload unmanned aerial vehicles (UAVs). Soybean Sci. **36**(1), 41–50 (2017)
12. Sarker, L.R., Nichol, J.E.: Improved for set biomass estimates using ALOS AVNIR-2 Texture indices. Remote Sens. Environ. **115**(4), 968–977 (2011)
13. Xu, T.: Method and application of forest biomass estimation based on LiDAR and OLI multispectral data. Nanjing Agricultural University, Jiangsu (2015)
14. Mu, Q.E., Gao, Z.H., Bao, Y.H., et al.: Estimation of sparse vegetation biomass based on Grey-Level Co-occurrence Matrix of vegetation indices. Remote Sens. Inf. **31**(1), 58–63 (2016)
15. Yue, J.B., Yang, G.J., Li, C.C., et al.: Estimation of winter wheat above-ground biomass using unmanned aerial vehicle-based snapshot hyperspectral sensor and crop height improved models. Remote Sens. **9**(70), 801–819 (2017)
16. Deng, S.B.: ENVI Remote Sensing Image Processing Method. Science Publishing, Beijing (2010)